Silicic ash beds bracket Emeishan Large Igneous province to < 1 m.y. at ~ 260 Ma

Article *in* Lithos · November 2016

DOI: 10.1016/j.lithos.2016.08.013

8 authors, including:

Huang Hu
Chengdu University of Technology
21 PUBLICATIONS **151** CITATIONS
SEE PROFILE

Peter Cawood
University of St Andrews
188 PUBLICATIONS **8,423** CITATIONS
SEE PROFILE

Yuansheng Du
China University of Geosciences
112 PUBLICATIONS **753** CITATIONS
SEE PROFILE

Lithos 264 (2016) 17–27

Contents lists available at ScienceDirect

Lithos

journal homepage: www.elsevier.com/locate/lithos

Silicic ash beds bracket Emeishan Large Igneous province to <1 m.y. at ~260 Ma

Hu Huang [a,b,*], Peter A. Cawood [b,c], Ming-Cai Hou [a], Jiang-Hai Yang [d], Shi-Jun Ni [e], Yuan-Sheng Du [d], Zhao-Kun Yan [a], Jun Wang [a]

[a] State Key Laboratory of Oil and Gas Reservoir Geology and Exploitation, Institute of Sedimentary Geology, Chengdu University of Technology, Chengdu 610059, China
[b] Department of Earth and Environmental Sciences, University of St. Andrews, St. Andrews KY16 9AL, UK
[c] Centre for Exploration Targeting, School of Earth and Environment, University of Western Australia, 35 Stirling Hwy, Crawley, WA 6009, Australia
[d] State Key Laboratory of Biogeology and Environmental Geology, China University of Geosciences, Wuhan 430074, China
[e] College of Earth Science, Chengdu University of Technology, Chengdu 610059, China

ARTICLE INFO

Article history:
Received 23 December 2015
Accepted 9 August 2016
Available online 18 August 2016

Keywords:
Geochemistry
Guadalupian—Lopingian boundary
Claystones
Emeishan
Silicic volcanism
Emeishan large igneous province

ABSTRACT

Claystone beds directly below and above the Emeishan basalts in SW China formed around the Guadalupian-Lopingian (G—L) boundary. Zircons from both levels give U–Pb ages of ~260 Ma, and are identical within-error to ages reported for the Emeishan Large Igneous Province (LIP). The claystones lack Nb—Ta anomalies on primitive mantle normalized elemental diagrams; zircons from these claystones have a geochemical affinity to within-plate-type magmas. These features, combined with the strong negative Eu anomalies in the zircons and high Al_2O_3/TiO_2 ratios, indicate that claystones around the G—L boundary have a silicic volcanic component related to Emeishan LIP. Zircons from the underlying claystone bed have much higher U/Yb and Th/Nb ratios and lower $\varepsilon_{Hf}(t)$ values than those overlying the LIP, suggesting that early-stage silicic volcanic rocks had a higher crustal contamination or assimilation during magmatic processes. In terms of stratigraphic correlation, our data demonstrate that silicic eruptions occurred not only at the end, but also at the beginning of the Emeishan LIP, and the overall duration of the main basaltic phase was short (<1 m.y).

1. Introduction

The Emeishan large igneous province (LIP) consists of voluminous basalts, picrites, mafic/ultramafic to felsic intrusions, as well as trachytes and rhyolites (Huang et al., 2014; Shellnutt, 2014; Xiao et al., 2004; Xu et al., 2001, 2010; Zhou et al., 2006) and has been dated at the Guadalupian—Lopingian (G—L) boundary (260 Ma) with a short eruption duration (<2 Ma) (Ali et al., 2002; Shellnutt et al., 2012; Zheng et al., 2010; Zhong et al., 2014; Zhou et al., 2002). Silicic volcanic rocks have only been reported from the uppermost levels of the volcanic successions (Anh et al., 2011; Shellnutt and Jahn, 2010; Xu et al., 2010) and are thought to represent the final stage of magmatic activity (He et al., 2007, 2010a; Xu et al., 2010; Zhong et al., 2014). Recent studies on derived Upper Permian sandstones that lie to the southeast of the Emeishan LIP indicate that the volume of associated silicic eruptions may have been underestimated (Yang et al., 2015). Such effusive activity may have played an important role in climate forcing associated with the LIP by releasing SO_2 into the stratosphere (Yang et al., 2015) and possibly link to the late Guadalupian (mid-Capitanian) mass extinction (Bond and Wignall, 2014; Bond et al., 2010; Day et al., 2015; Jerram et al., 2016; Zhang et al., 2013).

Across much of SW China claystone beds accumulated around the G—L boundary (Isozaki et al., 2004; Saitoh et al., 2013; Sun et al., 2010; Zhang et al., 2007) and although they have been invoked as providing a link between the mass extinction and volcanism (He et al., 2010a; Zhong et al., 2014), their source is disputed. For example, Isozaki et al. (2004) and Isozaki (2009) argued that claystones originated from acidic tuffs related to subduction of the Panthalassa Ocean, whereas He et al. (2010a) proposed that they were mudstones derived from the uppermost silicic member of the Emeishan LIP. In this paper, we present whole-rock geochemistry and zircon trace elements, U–Pb and Lu—Hf isotopic data on claystones directly underlying and overlying Emeishan basalts in SW China to determine their source and explore their implication for Emeishan LIP volcanism. We show that G—L boundary claystones have a silicic volcanic origin linked to the LIP, and that silicic volcanism occurred not only at the end, but also prior to the Emeishan LIP's emplacement and that the total duration of igneous activity was no more than 1 m.y.

* Corresponding author at: State Key Laboratory of Oil and Gas Reservoir Geology and Exploitation, Institute of Sedimentary Geology, Chengdu University of Technology, Chengdu 610059, China.
E-mail address: 118huanghu@163.com (H. Huang).

http://dx.doi.org/10.1016/j.lithos.2016.08.013
0024-4937/

2. Geological background and sampled stratigraphy

The Emeishan LIP covers an area of ~250,000 km^2 near the western margin of the Yangtze Block in SW China (Ali et al., 2005; Chung and Jahn, 1995; Xu et al., 2001) (Fig. 1; Ali et al., 2010). The volcanic succession ranges from a maximum preserved thickness of ~5 km in the west of the province to less than 100 m in the east (Xu et al., 2001). The Emeishan basalts overlie the limestone-dominated Middle Permian Maokou Formation, and are, in turn, partially covered by clastic rocks of the Upper Permian Xuanwei or Longtan formations in the east and Triassic sedimentary rocks in the centre (He et al., 2003; Yang et al., 2015).

In the northeastern Emeishan LIP, the volcanic pile is approximately 270 m thick and lies between the Maokou and Xuanwei formations. The lower and upper parts of the volcano-sedimentary successions are well preserved at the Qingyin Power Station and Qingyin Ge Temple, respectively (Fig. 2; Thompson et al., 2001). The uppermost part of the Maokou Formation at the Qing Yin Power Station consists of claystone-rich succession (Figs. 2, 3). The top of the Maokou limestones are marked by an irregular surface in which hollows are infilled with reddish-brown ferruginous mudstones (Fig. 4a) and minor yellow claystones known as the Wangpo Bed (~35 cm thick) (Lai et al., 2008). This in turn is overlain by the Heshan Bed (~1 m thick) (Lai et al., 2008), consisting of a thin succession of carbonaceous shales and limestones in which the uppermost of the shales is intercalated with thin red-brown ferruginous mudstone. The Heshan Bed is capped by the lowermost lava flow of the Emeishan LIP. Biostratigraphy indicates the limestones underlying the Wangpo Bed belong to the late Capitanian *J. xuanhanensis* zone (Fig. 3; Lai et al., 2008; Sun et al., 2010) corresponding to an absolute age of around 261 Ma (Henderson et al., 2012).

The uppermost Emeishan basalts at the Qingyin Ge Temple section are heavily altered (Thompson et al., 2001) and overlain by the Xuanwei Formation. The formation is approximately 96 m thick and composed of clastic rocks that accumulated in a terrestrial environment (He et al., 2007; Thompson et al., 2001). The basal Xuanwei Formation consists of yellow claystones ~0.7 m thick (Fig. 3) that represent tuffaceous rocks and are considered to mark the waning phase of volcanic activity associated with the LIP (Thompson et al., 2001). Iron-polymetallic deposits overlie the claystones with an irregular surface, and are, in turn, covered by dark-green sandstones (Fig. 4b).

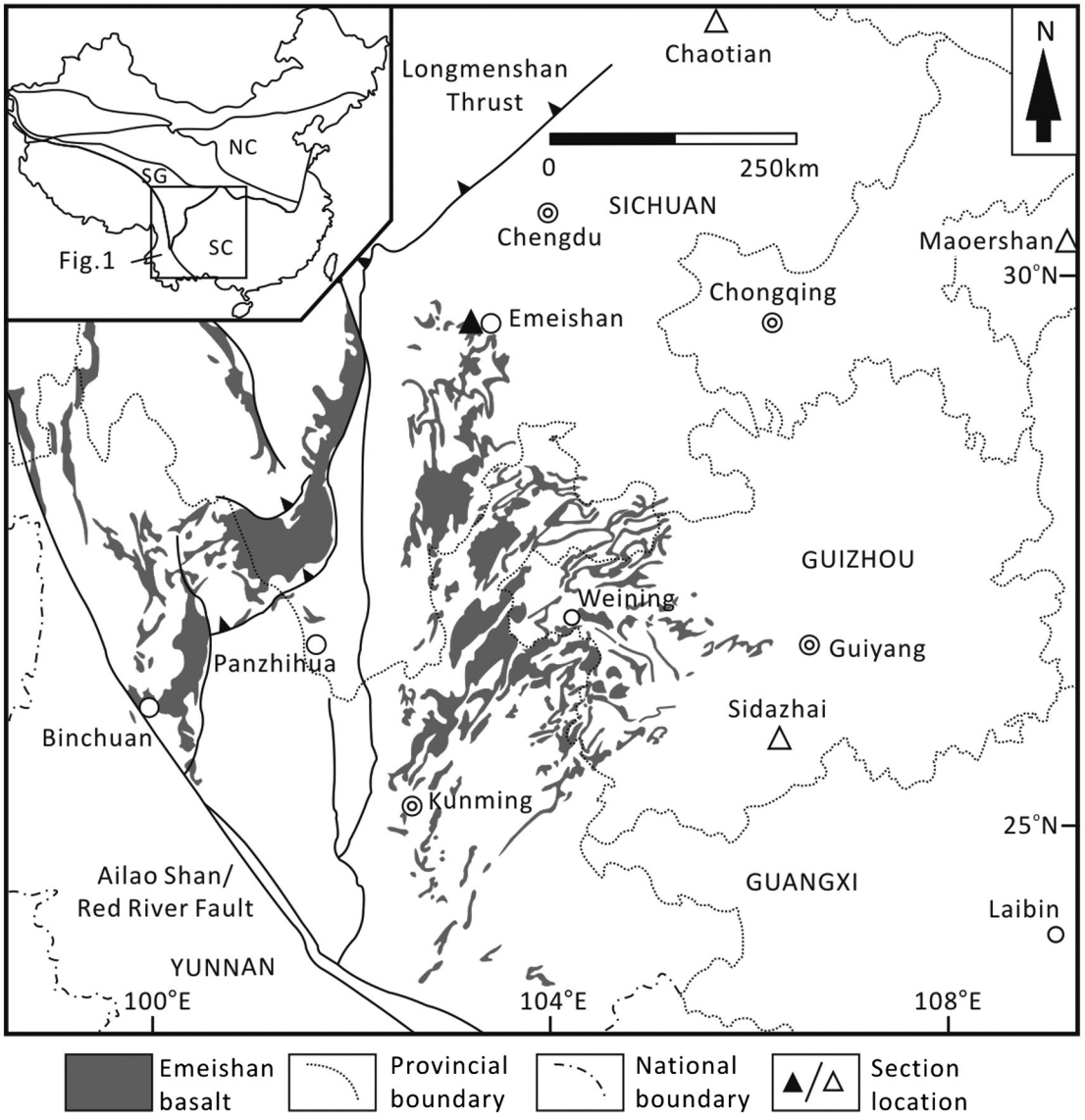

Fig. 1. Schematic map showing the distribution of the Emeishan basalts and the studied section locations (based on Ali et al., 2010). Also shown are the sections at Chaotian (He et al., 2010a; Saitoh et al., 2013), Maoershan (Zhang et al., 2007), and Sidazhai (Yang et al., 2015). SC, South China craton; SG, Songpan-Ganzi; and NC, North China craton.

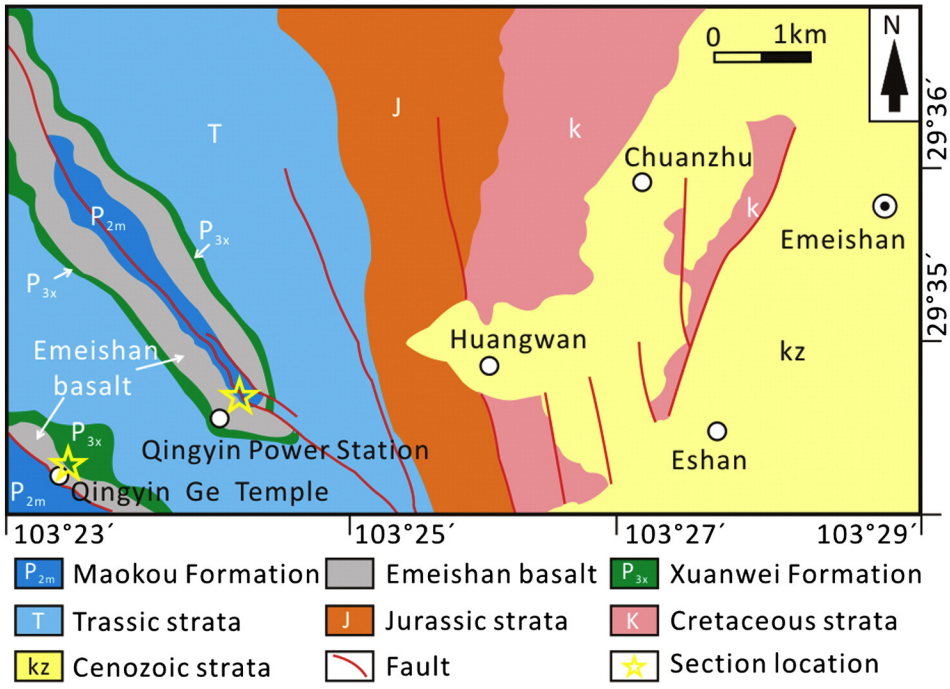

Fig. 2. Simplified geological map of the Qingyin area.

3. Samples and analytical methods

Fifteen volcano-sedimentary rock samples were analyzed for bulk-rock geochemistry, including two ferruginous mudstone samples and six claystone samples from the Wangpo Bed of the Maokou Formation and six claystone samples and one iron-polymetallic sample (Xw4) from the lowest Xuanwei Formation (Fig. 3). All samples were reduced in a corundum jaw crusher (to 60 mesh). About 60 g from each sample

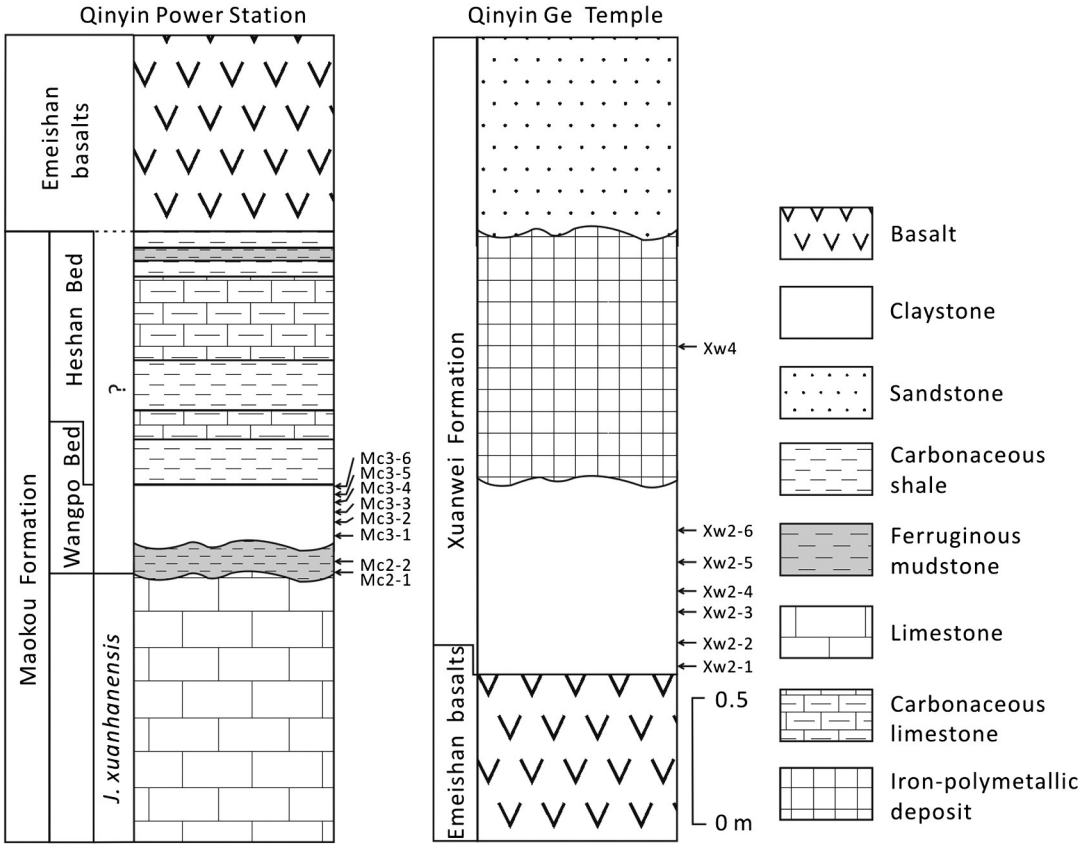

Fig. 3. Stratigraphic section and sampling locations at Qingyin. Biostratigraphic data for the Qinyin Power Station are from Sun et al. (2010).

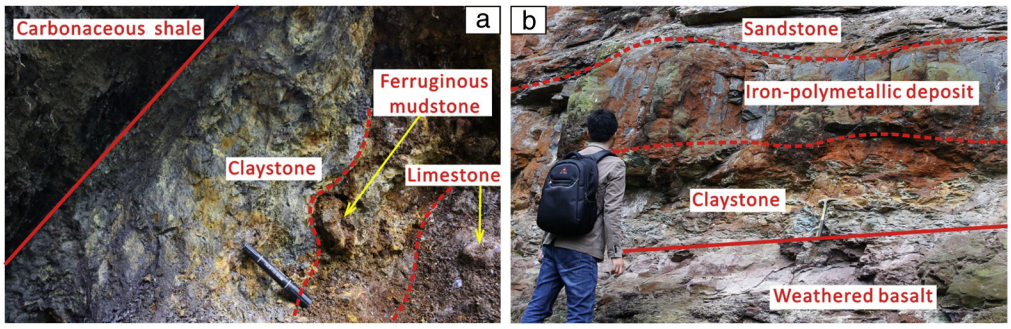

Fig. 4. Outcrop photographs of the Wangpo Bed (N: 29°34′42.7″; E: 103°24′39.2″) (a) and lowest Xuanwei Formation (N: 29°34′30.7″; E: 103°23′35.0″) (b). Mark pen (14 cm) for scale.

was powdered in an agate ring mill to less than 200 mesh. Major element concentrations were determined with XRF by ALS Chemex. Trace elements were analyzed at the State Key Laboratory of Geological Processes and Mineral Resources (GPMR), China University of Geosciences (Wuhan). The rock powers were first digested by HF + HNO_3 in Teflon bombs and analyzed with an Agilent 7500a ICP—MS. The detailed sample-digesting procedure for ICP—MS analyses is the same as described by Liu et al. (2008). For the trace element analysis, the standard reference materials were AGV-2 (andesite), BHVO-2 (basalt), BCR-2 (basalt) and GSR-1 (granite). The results of the standard analyses and the reference values are available in Supplementary Table 1. The analytical precisions are generally <5% for most major and trace elements.

Zircons for U–Pb dating and trace element analysis were extracted from claystone samples Mc3–2 and Xw2–4 and analyzed by LA—ICPMS at GPMR. Detailed operating conditions for the laser ablation system and the ICP—MS instrument and data reduction are the same as description by Liu et al. (2010). Zircon 91500 ($^{206}Pb/^{238}U$ age = 1062.4 ± 0.4 Ma, Wiedenbeck et al., 1995) was used as external standard for U–Pb dating, and was analyzed twice every six analyses. Off-line selection and integration of background and signals, and time-drift correction and quantitative calibration for trace element analyses and U–Pb dating were performed by ICPMSDataCal (Liu et al., 2010). Concordia diagrams and weighted mean age calculations were conducted using Isoplt/Ex_ver3.75 (Ludwig, 2003). Zircon standards Gj-1 was analyzed as an unknown and the obtained mean $^{206}Pb/^{238}U$ age is 599 ± 4 Ma (2σ) in line with the recommended age [599.8 ± 1.7 Ma (2σ), (Jackson et al., 2004)]. Trace element compositions of zircons were calibrated against reference materials BCR-2G and BIR-1G, combined with internal standardization (Liu et al., 2010). The preferred values of element concentrations for the USGS reference glasses are from the GeoReM database (http://georem.mpch-mainz.gwdg.de/). The average analytical error ranges from ca. ±10% for light rare earth elements (LREE) to ca. ±5% for the other REEs.

In situ zircon Lu—Hf isotopic analysis was carried out on a Neptune Plus MC—ICP—MS (Thermo Fisher Scientific, Germany) in combination with a Geolas 2005 excimer ArF laser ablation system (Lambda Physik, Göttingen, Germany) hosted at the GPMR. Analytical spots ware located close to, or on the top of, spots used for U–Pb analysis or in the same growth domain as inferred from CL images. Detailed operating conditions for the laser ablation system, the MC—ICP—MS instrument and analytical method are the same as outlined by Hu et al. (2012). The analyses were conducted with a beam diameter of 44 μm and a hit rate of 6 Hz. Zircon 91500 and GJ-1 were used as the reference standard. Off-line selection and integration analyte signals, and isobaric interference and mass fractionation correction of Lu–Hf isotopic ratios were also performed by ICPMSDataCal (Liu et al., 2010). The decay constant was adopted for ^{176}Lu of 1.865×10^{-11} $year^{-1}$ (Scherer et al., 2001). The value of $\varepsilon_{Hf}(t)$ is calculated relative to the chondritic reservoir with a $^{176}Hf/^{177}Hf$ ratio of 0.282772 and $^{176}Lu/^{177}Hf$ of 0.0332 (Blichert-Toft and Albarède, 1997).

4. Results

4.1. Major and trace elements

The whole-rock geochemical data for the analyzed samples are presented in Supplementary Table 2. The SiO_2 contents of the samples are highly variable (13.30 wt.% to 53.22 wt.%). The ferruginous mudstone and iron-polymetallic samples have extremely high Fe_2O_3 contents (40.63 wt%–57.66 wt%). Claystone samples from the lowermost Xuanwei Formation have higher Fe_2O_3 contents (5.35 wt%–15.11 wt%) than claystone samples from the Wangpo Bed. All claystone samples and the iron-polymetallic sample are characterized by high Al_2O_3 contents (19.86 wt%–35.13 wt%), reflecting the presence of abundant clay minerals.

The ferruginous mudstone samples have chondrite-normalized rare-earth element (REE) patterns with slightly positive Ce and negative Eu anomalies and a gradual decrease in REE (Fig. 5a). The claystone samples from the Wangpo Bed are characterized by light REE enrichment, significant negative Eu anomalies and fairly flat heavy REE pattern. All claystone samples and the iron-polymetallic sample from the Xuanwei Formation have flat REE patterns, along with significant positive Ce anomalies and slightly negative or no Eu anomalies (Fig. 5c). On primitive mantle-normalized plots, the ferruginous mudstone samples show significant negative Nb, Ta, Zr and Hf anomalies, which are absent from the other samples (Fig. 5b, d). Claystone samples from the Wangpo Bed have slightly positive Ti anomalies, which are lacking from other samples.

4.2. Zircon U–Pb ages

Zircon grains from samples Mc3–2 and Xw2–4 are generally prismatic with relatively uniform sizes (50–120 μm for Mc3–2 and 80–150 μm for Xw2–4). Cathodoluminescence (CL) imaging shows that most grains exhibit clear oscillatory zoning and a few grains display a homogenous internal structure (Fig. 6).

All analyzed zircon grains from sample Mc3–2 have high Th/U ratios (0.41–1.28) (Supplementary Table 3), indicating a magmatic origin (Hoskin and Schaltegger, 2003). Of the sixty-five zircon grains, two analyses (#4 and #17) are discordant [($^{206}Pb/^{238}U$) age /($^{207}Pb/^{235}U$) age < 0.9]. Twelve analyses are concordant, but six yield $^{206}Pb/^{238}U$ ages of 318–282 Ma, three yield $^{206}Pb/^{238}U$ ages of 869–752 Ma and three yield $^{207}Pb/^{206}Pb$ ages of 2166–1521 Ma, significantly older than the majority of the analyses (Supplementary Table 3). The remaining fifty-one concordant zircon grains define a tight age cluster with a mean $^{206}Pb/^{238}U$ age of 260.4 ± 1.2 Ma (2 σ) with a mean square of weighted deviate (MSWD) value of 0.96 (Fig. 7a). This weighted average age is equal to the concordia age within error [260.8 ± 2.0 Ma (2 σ, MSWD = 0.90)] calculated from the youngest nineteen analyses with concordance >96%.

For sample Xw2–4, fifty-two analyses were obtained from fifty-one zircon grains, of which forty-eight are concordant. All analyses have

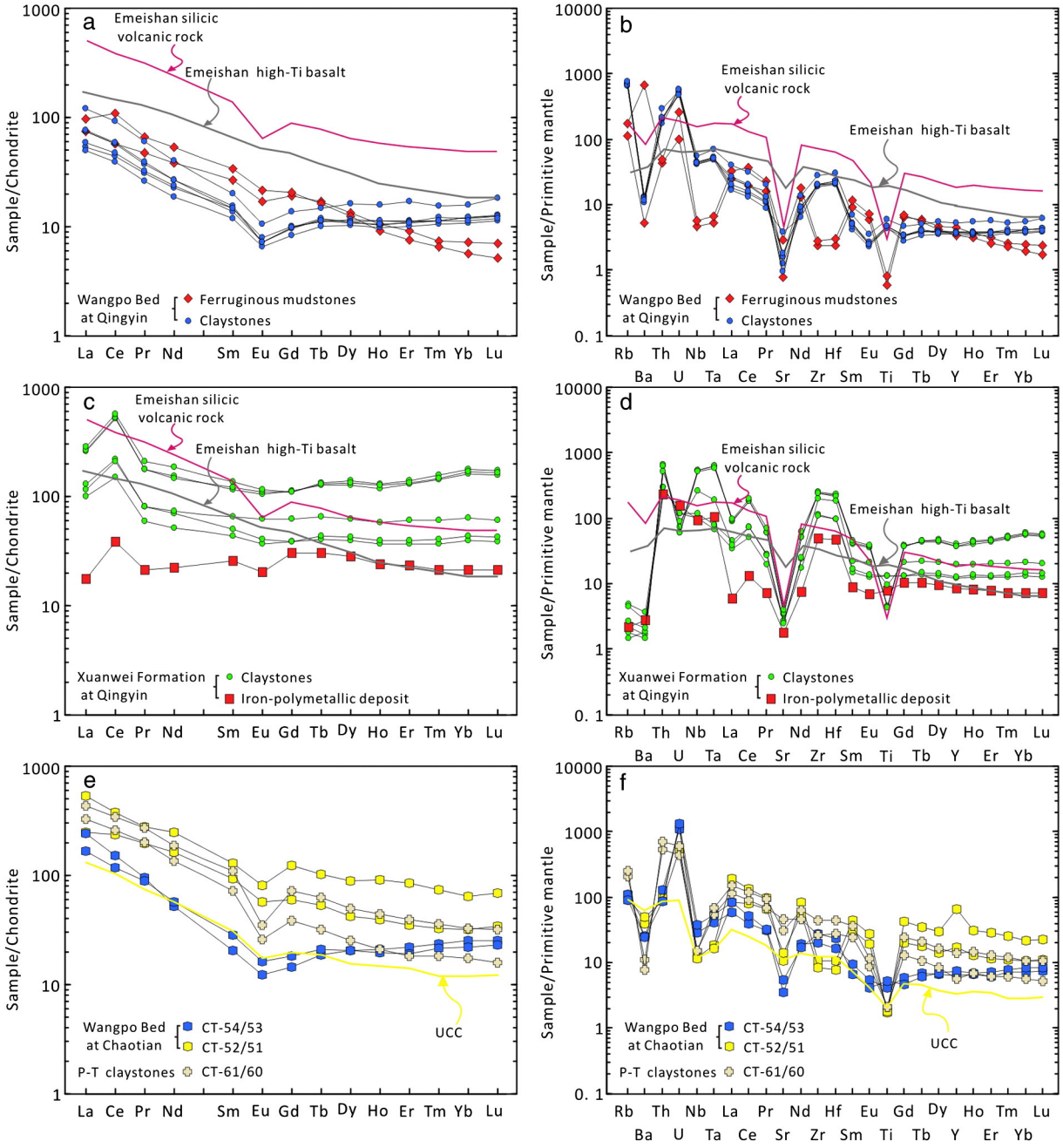

Fig. 5. Chondrite-normalized REE patterns distribution, and primitive mantle-normalized spidergrams for claystone samples at Qingyin (a, b, c, d) and Chaotian (e, f). Normalized values for chondrite and primitive mantle are from Sun and McDonough (1989). Date from claystones of the Wangpo Bed and around the P–T boundary at Chaotian are from He et al. (2010a). Average values of Emeishan high-Ti basalts at Binchuan (Xiao et al., 2004; Xu et al., 2001), Emeishan trachytes and rhyolites (Anh et al., 2011; Shellnutt and Jahn, 2010; Xu et al., 2010), and the average upper continental crust (UCC) (Rudnick and Gao, 2003) are shown for comparison.

high Th/U ratios (0.51–1.52) (Supplementary Table 3), indicating a magmatic origin (Hoskin and Schaltegger, 2003). Three concordant analyses on bright or dark cores and rims of core-rim structured zircons yield Precambrian ages ranging from 828 to 805 Ma. The remaining forty-five concordant analyses yield ages of 295–252 Ma, of which the youngest forty-one zircon grains give a weighted mean $^{206}Pb/^{238}U$ age of 260.4 ± 1.7 Ma (2 σ) with a MSWD value of 0.88 whereas the others yield slightly older ages (295–284 Ma) interpreted to represent earlier magmatic pulses (Fig. 7b). This weighted average age is equal to the concordia age within error [259.0 ± 2.8 Ma (2 σ, MSWD = 0.07)] calculated from the youngest thirteen analyses with concordance >95%.

4.3. Zircon trace elements

The chemical compositions for forty-three grains with ages in the range of 268–254 Ma ($^{206}Pb/^{238}U$ age) from sample Mc3–2 and twenty grains ranging in age from 266 to 253 Ma from sample Xw2–4 are presented in Supplementary Table 4. Most of the analyzed grains have REE's patterns that increase steeply from La to Lu, with positive Ce anomalies and negative Eu anomalies (Fig. 8). The composition of the zircon grains show an overall increase in Nb content, and a decrease in Hf content from sample Mc3–2 (most <10 ppm and 7189–10,509 ppm, respectively) to sample Xw2–4 (most >14 ppm and 6760–7917 ppm, respectively). The geochemistry of zircon provides a

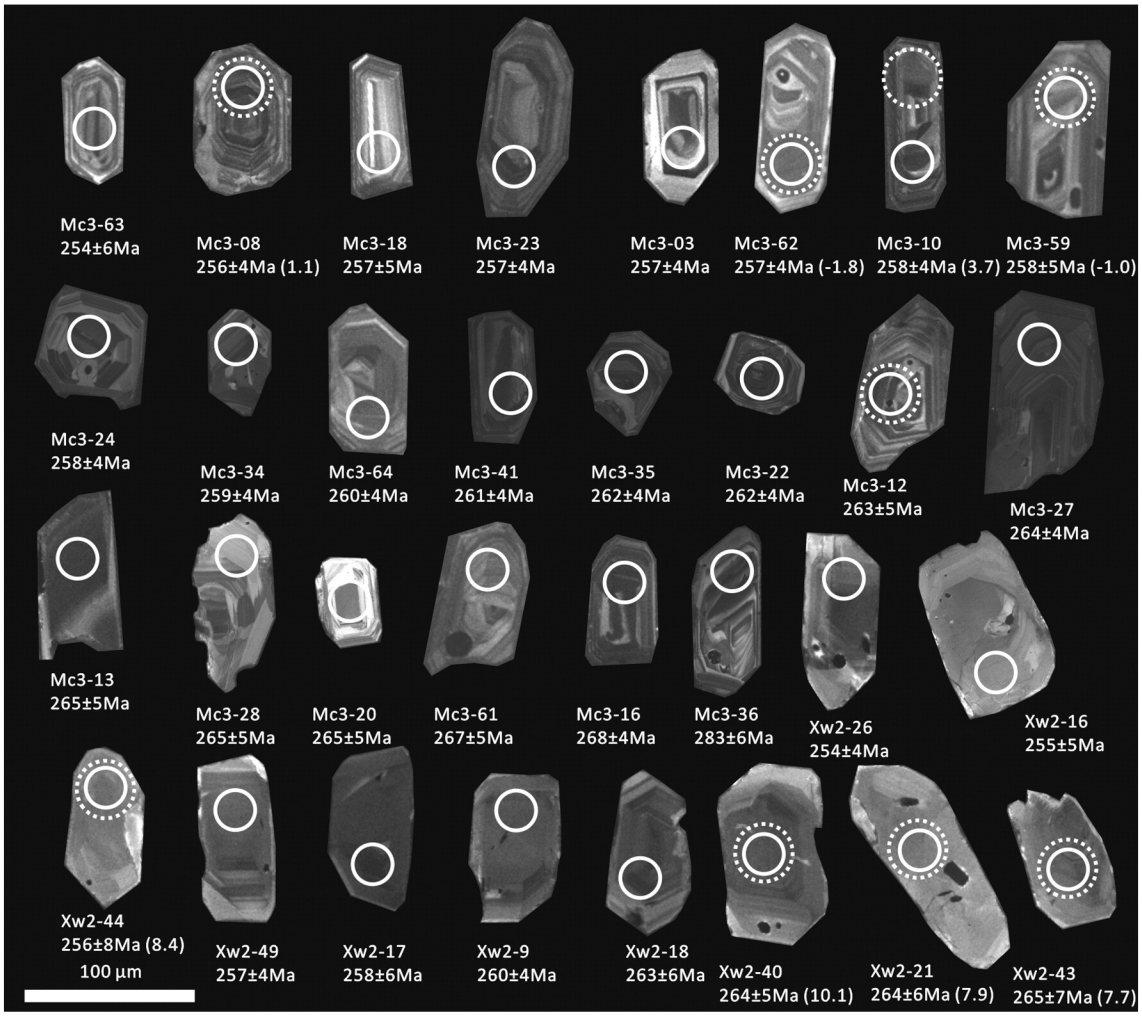

Fig. 6. Cathodoluminescence images for zircons from claystone samples Mc3–2 and Xw2–4 at Qingyin. The white solid and circles denote U–Pb and Lu–Hf spots, respectively. The numbers in the brackets on the right of the U–Pb ages are $\varepsilon_{Hf}(t)$ values.

sensitive monitor of its parental magma composition and is effective for fingerprinting tecto-magmatic provenance (Grimes et al., 2015). All zircons were plotted on Hf vs. U/Yb, and Th/Nb vs. Hf/Th diagrams (Fig. 9) to examine the nature of the source magma from which they crystallized (Grimes et al., 2015; Yang et al., 2012). The majority of the Permian zircons lie in the continental zircon and within-plate/anorogenic fields with a few falling into the arc-related/orogenic field (Fig. 9).

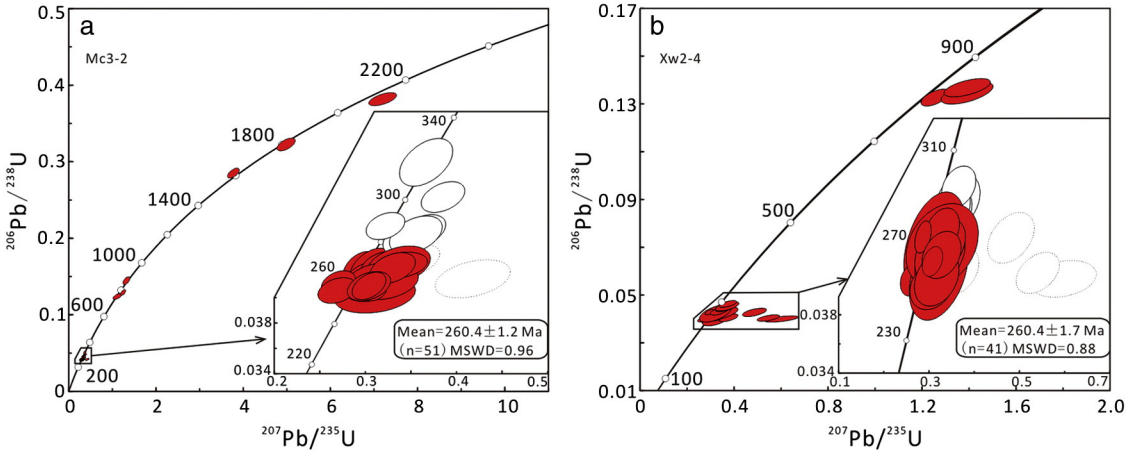

Fig. 7. LA–ICPMS zircon U–Pb concordia diagrams for claystone samples Mc3–2 and Xw2–4.

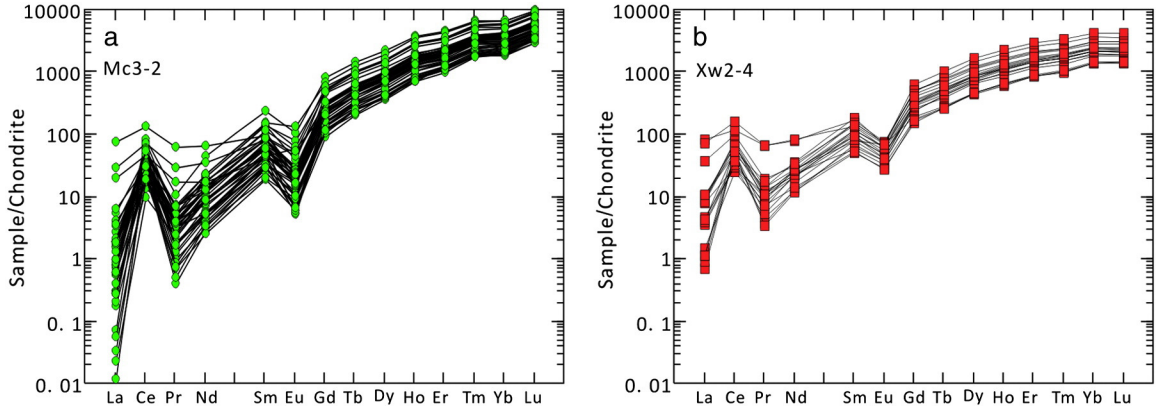

Fig. 8. Chondrite-normalized REE patterns for claystone samples Mc3–2 and Xw2–4. Normalized values for chondrite are from Sun and McDonough (1989).

4.4. Zircon Lu–Hf isotopes

The Lu–Hf isotopic compositions for seventeen grains with ages ~260 Ma from samples Mc3–2 and Xw2–4 are presented in Supplementary Table 5. Eleven analyses from sample XW2–4 yield relatively uniform $^{176}Hf/^{177}Hf$ ratios (0.282834–0.282939) and $\varepsilon_{Hf}(t)$ values (+7.7 to +11.5). However, six analyses from sample Mc3–2 exhibit a relatively lower $^{176}Hf/^{177}Hf$ ratio between 0.282567 and 0.282727 and $\varepsilon_{Hf}(t)$ values (−1.8 to +3.7) (Fig. 10).

5. Discussion

5.1. Intense chemical weathering

Chemical weathering leaches and subsequently depletes the soluble elements Ca, Na and K relative to Al and, in some cases, Fe (Fedo et al., 1995; Nesbitt and Young, 1982; Tosca et al., 2010). The degree of weathering is expressed by the chemical index of alteration (CIA). $CIA = [Al_2O_3 / (Al_2O_3 + CaO^* + Na_2O + K_2O)] \times 100$ in molecular proportions, where CaO^* represents CaO content in the silicate fraction (Nesbitt and Young, 1982). In the absence of the carbonate content and CO_2 data, it is difficult to accurately estimate the silicate CaO content. Therefore, to compute for silicate CaO content, the assumption proposed by Bock et al. (1998) was adopted. In this regard, CaO values were accepted only if $CaO < Na_2O$; if however, $CaO > Na_2O$ then we assumed that the moles of silicate $CaO = Na_2O$ (Bock et al., 1998). The calculated CIA values for the claystone and iron-polymetallic samples from the lowest Xuanwei Formation are approximately 99. Given the higher K_2O contents (1.16 wt%–8.10 wt%) for ferruginous mudstone and claystone samples from the Wangpo Bed, the lower CIA values (70–78) for these samples may be partially attributed to diagenetic K-metasomatism (Fedo et al., 1995). To mitigate the effects of K enrichment, Fedo et al. (1995) proposed the plagioclase index of alteration ($PIA = [(Al_2O_3 - K_2O) / (Al_2O_3 + CaO^* + Na_2O)] \times 100$), which is preferred for evaluation of the chemical weathering intensity of plagioclase. The calculated PIA values for all samples range between 97 and 99, indicating extreme weathering.

The iron-polymetallic deposits at Emeishan are characterized by a pisoid-ooid texture with a size range of 0.1 mm to 1.5 mm and are thought to have formed by chemical leaching during sedimentary processes in surface environments (Meng et al., 2015). Ce is more sensitive to change in redox conditions than other REEs in surface environments, and is generally preferentially precipitated from the solution as Ce oxides under oxic conditions (e.g., Ma et al., 2011). Furthermore, Fe is redox sensitive and in reducing environments, ferrous iron (Fe^{2+}) can be mobile and leached during mafic mineral weathering. In oxidative weathering environments, however, Fe is usually retained by the formation of highly insoluble ferric iron (Fe^{3+}) oxides or oxyhydroxides and thus enriched along with Al (Babechuk et al., 2014). All claystone samples from the lowest Xuanwei Formation show significant positive Ce anomalies and Fe_2O_3 enrichment, consistent with formation during long-term surface exposure-related weathering. The ferruginous mudstone samples show extremely high Fe_2O_3 contents and PIA values, and slight positive Ce anomalies, comparable to the claystones and iron-polymetallic deposits from the lowest Xuanwei Formation. Given

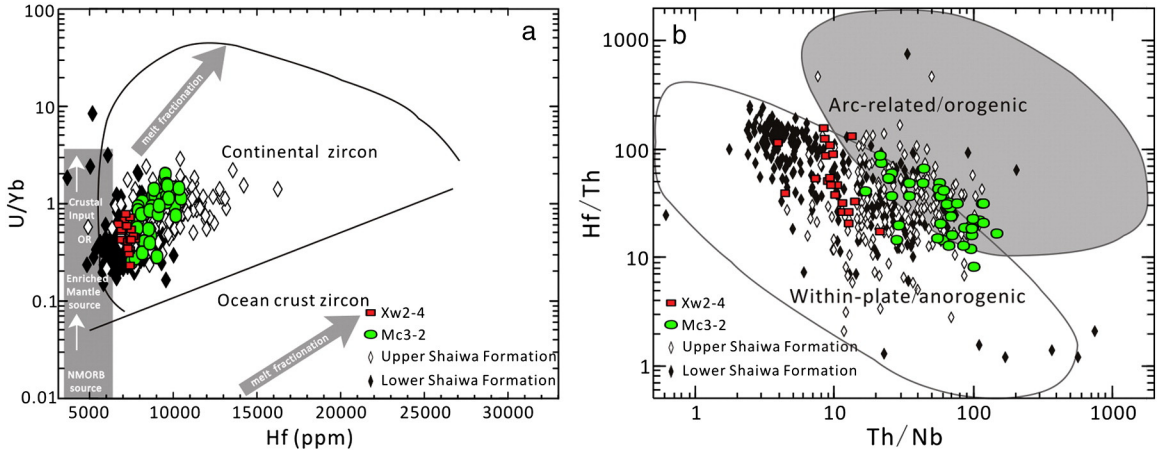

Fig. 9. Hf vs. U/Yb (Grimes et al., 2015) and Th/Nb vs. Hf/Th diagrams (Yang et al., 2012) for zircons of claystone samples Mc3–2 and Xw2–4. Dates from zircons in clastic rocks of the Upper Permian Shaiwa Formation at Sidazhai (Yang et al., 2015) are shown for comparison.

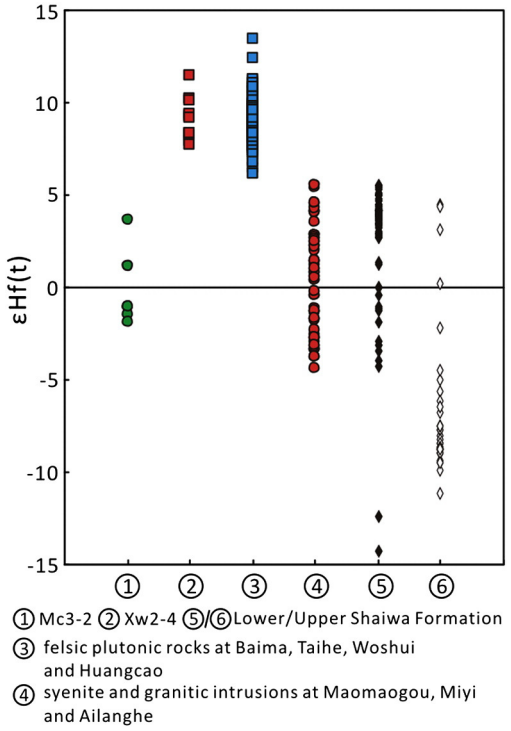

Fig. 10. Zircon $\varepsilon_{Hf}(t)$ values for the claystones of the Wangpo Bed and the lowest Xuanwei Formation at Qingyin, felsic plutonic rocks at Baima, Taihe, Woshui and Huangcao (Shellnutt et al., 2009), syenite and granitic intrusions at Maomaogou, Miyi and Ailanghe (Xu et al., 2008), and clastic rocks of the Upper Permian Shaiwa Formation at Sidazhai (Yang et al., 2015).

the irregular surface between the top of the limestones and the Wangpo Bed, these geochemical characteristics may be attributed to a long-term exposure, weathering and leaching at the base of the Wangpo Bed. This interpretation is also supported by the conodont studies at Maoershan (Fig. 1), where the Wangpo Bed are interbedded with limestones belonging to the latest Capitanian *C. postbitteri hongshuiensis* Zone (Fig. 11; Zhang et al., 2007), corresponding to two conodont zones higher than limestones underlying the Wangpo Bed at Qingyin. This potential gap in the conodont zones corresponds to a time break of around 1 Ma (Henderson et al., 2012). Long-term surface exposure may be related to the rapid regressive event during the mid-Capitanian (Sun et al., 2010; Wignall et al., 2009) or/and pre-eruption uplift of this LIP (Ali et al., 2010; He et al., 2003).

5.2. Origin of G–L boundary claystones

All claystone samples at the two analyzed sections lack Nb (Ta) anomalies on primitive mantle-normalized trace element diagrams (Fig. 5b, d), which is similar to the Emeishan high-Ti basaltic rocks and silicic volcanic rocks (Fan et al., 2008; Xiao et al., 2004; Xu et al., 2001, 2010), and contrast with upper continental crust which display such anomalies (Rudnick and Gao, 2003). Claystone samples from the Wangpo Bed and lowest Xuanwei Formation have ages (~260 Ma) comparable to the age of magmatic activity of the Emeishan LIP (He et al., 2007; Xu et al., 2008; Zhong et al., 2014; Zhou et al., 2002), suggesting a genetic link. Importantly, the trace element patterns of zircons with ages of ~260 Ma mostly fall in the continental zircon and within-plate/anorogenic fields (Fig. 9), consistent with an Emeishan LIP source (Chung and Jahn, 1995; Xiao et al., 2004; Xu et al., 2001; Yang et al., 2012, 2014). Given the generally zircon-poor or barren nature of basaltic rocks, the presence of abundant euhedral zircons with ages of ~260 Ma suggests that the claystones were mainly related to silicic eruptions. The high Al_2O_3/TiO_2 ratios of the analyzed samples, as well as the strong negative Eu anomalies (generally <0.25) in the zircons are consistent with a silicic rather than a basaltic source (He et al., 2007; Yang et al., 2015).

The Wangpo claystone bed overlies limestones of the Maokou Formation and lies directly beneath the Emeishan basalts or, where the basalts are absent, the limestones of the Upper Permian Wuchiaping Formation (Fig. 11; Lai et al., 2008; Saitoh et al., 2013). The Wangpo claystones have traditionally been considered to represent terrigenous shales related to a major regression event across western South China (Mei et al., 1994). A primary clastic composition for the claystones has been justified in part on the basis of their high quartz content as well their Al_2O_3/TiO_2 ratios (13–39) and Eu/Eu^* values (0.64–0.74), which are lower and higher respectively, than claystones from the Permian–Triassic (P–T) boundary, which originated from acidic tuffs (He et al., 2010a). However, compositional differences between the two sequences likely reflect a different composition for the volcanic activity rather than a non-volcanic source of the Wangpo claystones. On the Nb/Y vs. Zr/TiO_2 diagram (Fig. 12a; Winchester and Floyd, 1977), the P–T boundary claystones have a geochemical affinity to rhyodacite/dacite, whereas those of the Wangpo claystones are comparable to Emeishan trachytes, which have lower Al_2O_3/TiO_2 ratios (mostly <23) and higher Eu/Eu^* values (mostly >0.55) than Emeishan rhyolites (Anh et al., 2011; Shellnutt and Jahn, 2010; Xu et al., 2010) (Fig. 12b). Isozaki et al. (2004) also supported a volcanic origin for the Wangpo Bed by identifying high temperature quartz.

Claystone samples (CT-51 and CT-52) from the lower part of the Wangpo Bed at Chaotian (Fig. 1; He et al., 2010a) show similar geochemical features to the upper continental crust and ferruginous mudstones at Qingyin (Fig. 5), indicative of derivation from the old continental crust. In addition, the clay mineralogy of the bed suggests input from detrital as well as a volcanic source (Deconinck et al., 2014). Inputs of old continental material may account for the high quartz contents in the claystones. Thus, we conclude that the claystones originated mainly from a silicic volcanic ash related to Emeishan volcanism in addition to a component of terrigenous-derived clastic material.

5.3. Implications for the silicic volcanism of the LIP

Silicic volcanic rocks including rhyolite and trachyte have only been reported from the top of the Emeishan volcanic succession and are restricted to specific locations (e.g., Binchuan and Panzhihua, Fig. 1; Shellnutt and Jahn, 2010; Xu et al., 2010). However, recent studies on derived Upper Permian sandstones at Sidazhai suggest that silicic eruptions of the Emeishan LIP may have been significantly underestimated (Yang et al., 2015). The limited present-day exposure of silicic volcanic rocks reflects their dispersal due to the likely explosive nature of the silicic volcanic activity as well as their preferential erosion relative to basaltic phases due to their position at the top of the succession (Yang et al., 2015). Meanwhile, previous studies on the G–L boundary claystones focused on the Chaotian area in the northeast of the LIP where the Emeishan basalts are absent (He et al., 2007, 2010a), which also limits the ability to constrain the volcanic sequence. It is clear that Emeishan basalts lie between the claystones from the Wangpo Bed and the lowest Xuanwei Formation at Qingyin (Fig. 3). Geochemical and zircon trace element and U–Pb age data on these claystones suggests they were derived from LIP silicic magmatism and that this volcanism occurred both before and after the main phase of basaltic eruptive activity.

Previous zircon Hf isotope studies of Emeishan LIP felsic plutonic rocks show variable $\varepsilon_{Hf}(t)$ values (−4.4 to +13.5) (Shellnutt et al., 2009; Xu et al., 2008). Zircons of claystones from the lowest Xuanwei Formation exhibit relatively high $\varepsilon_{Hf}(t)$ values (>+7), comparable with those from felsic plutonic rocks (Fig. 10; Baima, Taihe, Woshui and Huangcao). This suggests that the late-stage silicic magmas were derived from melting of a mantle source without significant crustal

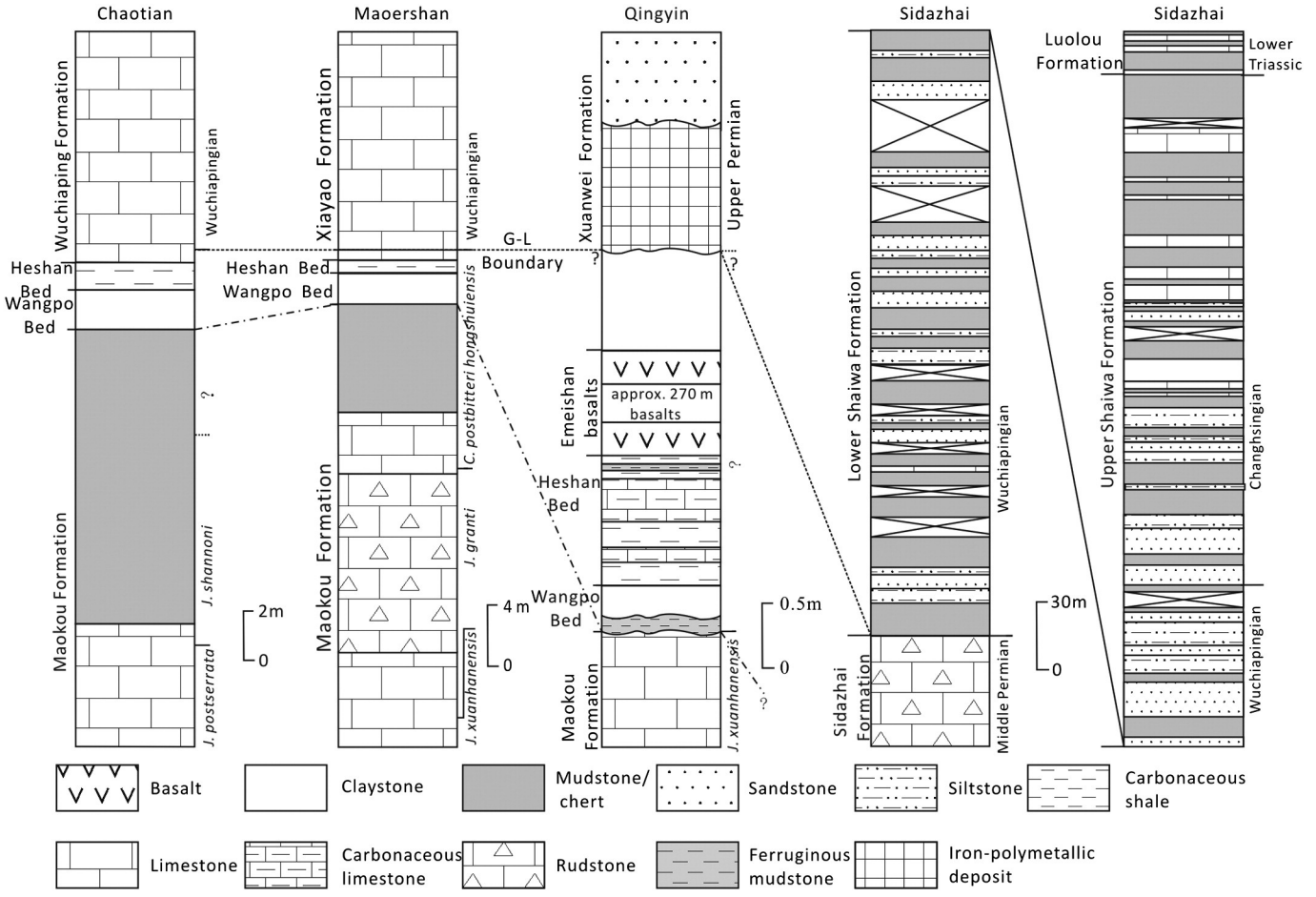

Fig. 11. Stratigraphic correlation among the Chaotian (Saitoh et al., 2013), Maoershan (Sun et al., 2010; Zhang et al., 2007), Qingyin (Sun et al., 2010; this study), and Sidazhai (Yang et al., 2015) sections. The dashed line represents the G–L boundary. The dashed and dot line at the base of the Wangpo Bed represents the possible isochron horizon.

contamination (Shellnutt et al., 2009; Xu et al., 2008). Zircons from the Wangpo claystones have lower $\varepsilon_{Hf}(t)$ values (−1.8 to +3.7), which are similar to ~260 Ma zircons from syenite and granitic intrusions at Maomaogou, Miyi and Ailanghe in the center of the LIP (Fig. 10; Xu et al., 2008). Such isotopic characteristics indicate a different magmatic process for zircons of claystones from the lowest Xuanwei Formation and suggest precipitation from more differentiated magmas with some involvement of crustal melting (Xu et al., 2008; Yang et al., 2015).

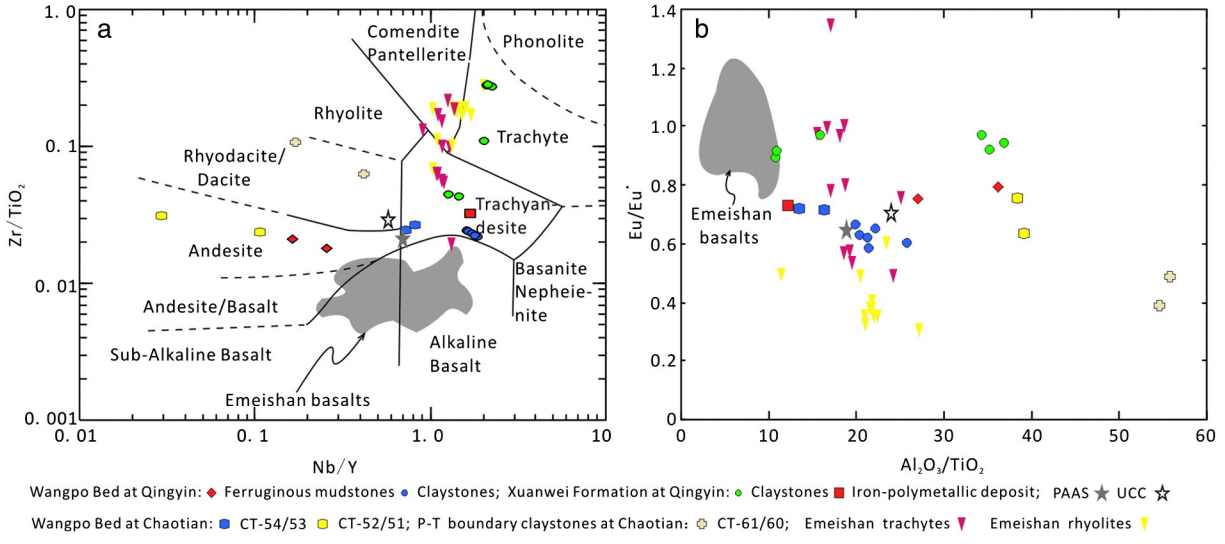

Fig. 12. (a) Nb/Y vs. Zr/TiO_2 (Winchester and Floyd, 1977) and (b) Al_2O_3/TiO_2 vs. Eu/Eu^*. Date from claystones of the Wangpo Bed and around the P–T boundary at Chaotian (He et al., 2010a), Emeishan basalts (Fan et al., 2008; He et al., 2010b; Qi et al., 2008; Xiao et al., 2003, 2004; Xu et al., 2001), Emeishan trachytes and rhyolites (Anh et al., 2011; Shellnutt and Jahn, 2010; Xu et al., 2010), the average upper continental crust (UCC) (Rudnick and Gao, 2003) and post-Archean average Australian shale (PAAS) (Taylor and McLennan, 1985) are shown for comparison.

Clastic rocks of the Upper Permian Shaiwa Formation at Sidazhai (Figs. 1, 11) were derived the Emeishan LIP and indicate a source composing ~30% silicic and ~70% basaltic rocks (Yang et al., 2015). Zircons of clastic rocks from the lower Shaiwa Formation have approximately lower U/Yb and Th/Nb ratios and higher $\varepsilon_{Hf}(t)$ values than those from the upper part (Figs. 9, 10), which suggests a reduction of crustal contamination or assimilation associated with Emeishan LIP magmatic source (Yang et al., 2015). Zircons of claystones from the lowest Xuanwei Formation have U/Yb (<0.8) and Th/Nb (<10) ratios comparable with those from the lower Shaiwa Formation (Fig. 9; Yang et al., 2015), suggesting that the derivation of the lowest Xuanwei claystones were related to the late-stage silicic volcanism of the Emeishan LIP. Zircons from the Wangpo claystones have higher $\varepsilon_{Hf}(t)$ values, though largely overlapping in U/Yb and Th/Nb ratios (Figs. 9, 10), than those from the upper samples of the Shaiwa Formation (Yang et al., 2015). Such chemical and isotopic characteristics suggest that silicic magmas derived from a source with more crustal contamination once existed elsewhere in the early stage of Emeishan volcanism.

5.4. Age constraints on the Emeishan LIP

More than 50 published zircon U–Pb ages for intrusive and extrusive rocks from the Emeishan LIP range from ~266 Ma to ~255 Ma (Shellnutt, 2014 and references therein). The distribution of most zircon U–Pb ages cluster around ~260 Ma (e.g. Fan et al., 2008; Xu et al., 2008; Zhou et al., 2002, 2006). However, most previous dating has been on the spot locations within the LIP. The coincident ages (ca. 260 Ma) of zircons from the claystone beds directly both below and above the Emeishan basalts suggest a relatively short time between silicic eruptions around the G–L boundary. Eruption of the main phase of Emeishan basaltic activity was thought to begin in the late Capitanian *J. xuanhanensis* zone, based on the conodont age dating the Maokou Formation limestones at Qingyin (Sun et al., 2010). However, our studies suggest that a long-term exposure may exist between the Wangpo Bed and the Maokou Formation limestones at Qingyin. The Wangpo Bed was formed in the latest Capitanian *C. postbitteri hongshuiensis* Zone (Fig. 11; Zhang et al., 2007), corresponding to an absolute age of around 260 Ma (Henderson et al., 2012), which constrains the age of early-stage basaltic volcanism of the Emeishan LIP. The high precision zircon CA-TIMS U–Pb age from the silicic extrusive rocks intercalated within the uppermost part of the high-Ti basalts at Binchuan is 259.1 ± 0.5 Ma. If this age represents the termination age of the Emeishan basalts (Zhong et al., 2014), then the overall duration of basaltic magmatism was short and probably <1 Ma. This interpretation is supported by the lack of palaeosols/intensely weathered flow tops between individual flows at Qingyin (Thompson et al., 2001).

6. Conclusions

Claystones around the G–L boundary at Qingyin directly underlie and overlie Emeishan basalts and formed during long-term surface exposure. Whole-rock geochemistry and zircon U–Pb ages and trace elements suggest that these claystones have a silicic volcanic origin related to the Emeishan LIP. Emeishan silicic volcanism occurred not only at the end, but also at the beginning, LIP magmatic activity. Zircons from claystones of the lowest Xuanwei Formation, which lie above the main pulse of basaltic magmatism have much higher $\varepsilon_{Hf}(t)$ values than those from the Wangpo claystones, which underlie the basalts. This indicates that Emeishan silicic magmas were derived from a source with decreasing crustal contamination. Combined with the biostratigraphic correlation, the coincident ages (ca. 260 Ma) of zircons from the claystone beds suggest a relatively rapid (<1 m.y.) emplacement of the terrain.

Supplementary data to this article can be found online at http://dx.doi.org/10.1016/j.lithos.2016.08.013.

Acknowledgements

We would like to thank Jason Ali, an anonymous reviewer and Editor Andrew Kerr, for their constructive comments and suggestions which substantially improved our manuscript. This research was supported by the Open Fund (PLC201404) of State Key Laboratory of Oil and Gas Reservoir Geology and Exploitation (Chengdu University of Technology), the National Natural Science Foundation of China (41502109), Project funded by China Postdoctoral Science Foundation (2015M582528) and the Fundamental Research Funds for the Central Universities, Chengdu University of Technology. We are grateful to Jiang-Hong Deng, Wen-Guang Yang, Xin-Chun Liu and Fu-Hao Xiong for help during the field work and Zhao-Chu Hu for his help with zircon U–Pb and Lu–Hf isotopic analysis.

References

Ali, J.R., Thompson, G.M., Song, X.Y., Wang, Y.L., 2002. Emeishan basalts (SW China) and the 'end-Guadalupian' crisis: magnetobiostratigraphic constraints. Journal of the Geological Society, London 159, 21–29.
Ali, J.R., Thompson, G.M., Zhou, M.F., Song, X., 2005. Emeishan large igneous province, SW China. Lithos 79, 475–489.
Ali, J.R., Fitton, J.G., Herzberg, C., 2010. Emeishan large igneous province (SW China) and the mantle-plume up-doming hypothesis. Journal of the Geological Society, London 167, 953–959.
Anh, T.V., Pang, K.N., Chung, S.L., Lin, H.M., Hoa, T.T., Anh, T.T., Yang, H.J., 2011. The Song Da magmatic suite revisited: a petrologic, geochemical and Sr–Nd isotopic study on picrites, flood basalts and silicic volcanic rocks. Journal of Asian Earth Sciences 42, 1341–1355.
Babechuk, M.G., Widdowson, M., Kamber, B.S., 2014. Quantifying chemical weathering intensity and trace element release from two contrasting basalt profiles. Deccan Traps, India, Chemical Geology 363, 56–75.
Blichert-Toft, J., Albarède, F., 1997. The Lu–Hf isotope geochemistry of chondrites and the evolution of the mantle–crust system. Earth and Planetary Science Letters 148, 243–258.
Bock, B., McLennan, S.M., Hanson, G.N., 1998. Geochemistry and provenance of the middle Ordovician Austin Glen member (Normanskill formation) and the Taconian orogeny in New England. Sedimentology 45, 635–655.
Bond, D.P., Wignall, P.B., 2014. Large igneous provinces and mass extinctions: an update. Geological Society of America Special Papers 505, 29–55.
Bond, D.P., Hilton, J., Wignall, P.B., Ali, J.R., Stevens, L.G., Sun, Y., Lai, X., 2010. The Middle Permian (Capitanian) mass extinction on land and in the oceans. Earth-Science Reviews 102, 100–116.
Chung, S.L., Jahn, B.M., 1995. Plume–lithosphere interaction in generation of the Emeishan flood basalts at the Permian–Triassic boundary. Geology 23, 889–892.
Day, M.O., Ramezani, J., Bowring, S.A., Sadler, P.M., Erwin, D.H., Abdala, F., Rubidge, B.S., 2015. When and how did the terrestrial mid-Permian mass extinction occur? Evidence from the tetrapod record of the Karoo Basin, South Africa. Proceedings of the Royal Society B 282, 20150834.
Deconinck, J.F., Crasquin, S., Bruneau, L., Pellenard, P., Baudin, F., Feng, Q., 2014. Diagenesis of clay minerals and K-bentonites in Late Permian/Early Triassic sediments of the Sichuan Basin (Chaotian section, Central China). Journal of Asian Earth Sciences 81, 28–37.
Fan, W.M., Zhang, C.H., Wang, Y.J., Guo, F., Peng, T.P., 2008. Geochronology and geochemistry of Permian basalts in western Guangxi Province, Southwest China: evidence for plume–lithosphere interaction. Lithos 102, 218–236.
Fedo, C.M., Nesbitt, H.W., Young, G.M., 1995. Unraveling the effects of potassium metasomatism in sedimentary rocks and paleosols, with implications for paleoweathering conditions and provenance. Geology 23, 921–924.
Grimes, C.B., Wooden, J.L., Cheadle, M.J., John, B.E., 2015. "Fingerprinting" tectono-magmatic provenance using trace elements in igneous zircon. Contributions to Mineralogy and Petrology 170, 1–26.
He, B., Xu, Y.G., Chung, S.L., Xiao, L., Wang, Y., 2003. Sedimentary evidence for a rapid, kilometer-scale crustal doming prior to the eruption of the Emeishan flood basalts. Earth and Planetary Science Letters 213, 391–405.
He, B., Xu, Y.G., Huang, X.L., Luo, Z.Y., Shi, Y.R., Yang, Q.J., Yu, S.Y., 2007. Age and duration of the Emeishan flood volcanism, SW China: geochemistry and SHRIMP zircon U–Pb dating of silicic ignimbrites, post-volcanic Xuanwei Formation and clay tuff at the Chaotian section. Earth and Planetary Science Letters 255, 306–323.
He, B., Xu, Y.G., Zhong, Y.T., Guan, J.P., 2010a. The Guadalupian–Lopingian boundary mudstones at Chaotian (SW China) are clastic rocks rather than acidic tuffs: implication for a temporal coincidence between the end-Guadalupian mass extinction and the Emeishan volcanism. Lithos 119, 10–19.
He, Q., Xiao, L., Balta, B., Gao, R., Chen, J., 2010b. Variety and complexity of the Late-Permian Emeishan basalts: reappraisal of plume–lithosphere interaction processes. Lithos 119, 91–107.
Henderson, C.M., Davydiv, V.I., Wardlaw, B.R., 2012. The Permian period. In: Gradstein, F.M., Ogg, J.M., Schmidt, M.D., Ogg, G. (Eds.), The Geologic Time Scale. Elsevier, pp. 653–680.
Hoskin, P.W.O., Schaltegger, U., 2003. The composition of zircon and igneous and metamorphic petrogenesis. Reviews in Mineralogy and Geochemistry 53, 27–62.

Hu, Z.C., Liu, Y.S., Gao, S., Liu, W.G., Zhang, W., Tong, X.R., Lin, L., Zong, K.Q., Li, M., Chen, H.H., 2012. Improved in situ Hf isotope ratio analysis of zircon using newly designed X skimmer cone and jet sample cone in combination with the addition of nitrogen by laser ablation multiple collector ICP–MS. Journal of Analytical Atomic Spectrometry 27, 1391–1399.

Huang, H., Du, Y.S., Yang, J.H., Zhou, L., Hu, L.S., Huang, H.W., Huang, Z.Q., 2014. Origin of Permian basalts and clastic rocks in Napo, Southwest China: implications for the erosion and eruption of the Emeishan large igneous province. Lithos 208-209, 324–338.

Isozaki, Y., 2009. Integrated "plume winter" scenario for the double-phased extinction during the Paleozoic–Mesozoic transition: the G-LB and P-TB events from a Panthalassan perspective. Journal of Asian Earth Sciences 36, 459–480.

Isozaki, Y., Yao, J., Matsuda, T., Sakai, H., Ji, Z., Shimizu, N., Kobayashi, N., Kawahata, H., Nishi, H., Takano, M., 2004. Stratigraphy of the Middle-Upper Permian and Lowermost Triassic at Chaotian, Sichuan, China Record of Late Permian double mass extinction event. Proceedings of the Japan Academy, Series B 80, 10–16.

Jackson, S.E., Pearson, N.J., Griffin, W.L., Belousova, E.A., 2004. The application of laser ablation–inductively coupled plasma–mass spectrometry to in situ U–Pb zircon geochronology. Chemical Geology 211, 47–69.

Jerram, D.A., Widdowson, M., Wignall, P.B., Sun, Y., Lai, X., Bond, D.P., Torsvik, T.H., 2016. Submarine palaeoenvironments during Emeishan flood basalt volcanism, SW China: implications for plume–lithosphere interaction during the Capitanian, Middle Permian ('end Guadalupian') extinction event. Palaeogeography, Palaeoclimatology, Palaeoecology 441, 65–73.

Lai, X.L., Wang, W., Wignall, P.B., Bond, D., Jiang, H.S., Ali, J.R., John, E.H., Sun, Y.D., 2008. Palaeoenvironmental change during the end-Guadalupian (Permian) mass extinction in Sichuan, China. Palaeogeography, Palaeoclimatology, Palaeoecology 269, 78–93.

Liu, Y.S., Zong, K.Q., Kelemen, P.B., Gao, S., 2008. Geochemistry and magmatic history of eclogites and ultramafic rocks from the Chinese continental scientific drill hole: subduction and ultrahigh-pressure metamorphism of lower crustal cumulates. Chemical Geology 247, 133–153.

Liu, Y.S., Gao, S., Hu, Z.C., Gao, C.G., Zong, K.Q., Wang, D.B., 2010. Continental and oceanic crust recycling-induced melt-peridotite interactions in the Trans-North China Orogen: U–Pb dating, Hf isotopes and trace elements in zircons from mantle xenoliths. Journal of Petrology 51, 537–571.

Ludwig, K.R., 2003. User's Manual for Isoplot 3.00: A Geochronological Toolkit for Microsoft Excel. Berkeley Geochronology Center, California, Berkeley (39 pp.).

Ma, L., Jin, L., Brantley, S.L., 2011. How mineralogy and slope aspect affect REE release and fractionation during shale weathering in the Susquehanna/Shale Hills Critical Zone Observatory. Chemical Geology 290, 31–49.

Mei, S., Jin, Y., Wardlaw, B.R., 1994. Zonation of conodonts from the Maokouan-Wuchiapingian boundary strata, South China. Palaeoworld 4, 225–233.

Meng, C.Z., Chen, Y., Zhang, Y.H., Wu, H., Ling, W.L., Zhang, H., Liu, J., 2015. Genetic relationship between unroofing of the Emeishan large igneous province and the iron-polymetallic deposit in western Guizhou, Southwestern China: constraint from U–Pb geochronology and geochemistry of zircon. Science China Earth Sciences 58, 1939–1950.

Nesbitt, H.W., Young, G.M., 1982. Early Proterozoic climates and plate motions inferred from major element chemistry of lutites. Nature 299, 715–717.

Qi, L., Wang, C.Y., Zhou, M.F., 2008. Controls on the PGE distribution of Permian Emeishan alkaline and peralkaline volcanic rocks in Longzhoushan, Sichuan Province, SW China. Lithos 106, 222–236.

Rudnick, R.L., Gao, S., 2003. Composition of the continental crust. In: Rudnick, R.L. (Ed.) Treatise on geochemistry 3, pp. 1–64.

Saitoh, M., Isozaki, Y., Yao, J., Ji, Z., Ueno, Y., Yoshida, N., 2013. The appearance of an oxygen-depleted condition on the Capitanian disphotic slope/basin in South China: Middle–Upper Permian stratigraphy at Chaotian in northern Sichuan. Global and Planetary Change 105, 180–192.

Scherer, E., Münker, C., Mezger, K., 2001. Calibration of the lutetium–hafnium clock. Science 293, 683–687.

Shellnutt, J.G., 2014. The Emeishan large igneous province: a synthesis. Geoscience Frontiers 5, 369–394.

Shellnutt, J.G., Jahn, B.M., 2010. Formation of the Late Permian Panzhihua plutonic-hypabyssal-volcanic igneous complex: implications for the genesis of Fe–Ti oxide deposits and A-type granites of SW China. Earth and Planetary Science Letters 289, 509–519.

Shellnutt, J.G., Wang, C.Y., Zhou, M.F., Yang, Y., 2009. Zircon Lu–Hf isotopic composi-tions of metaluminous and peralkaline A-type granitic plutons of the Emeishan large igneous province (SW China): constraints on the mantle source. Journal of Asian Earth Sciences 35, 45–55.

Shellnutt, J.G., Denyszyn, S.W., Mundil, R., 2012. Precise age determination of mafic and felsic intrusive rocks from the Permian Emeishan large igneous province (SW China). Gondwana Research 22, 118–126.

Sun, S.S., McDonough, W.F., 1989. Chemical and isotopic systematics of oceanic basalts: implications for mantle composition and processes. Geological Society London Special Publications 42, 313–345.

Sun, Y.D., Lai, X.L., Wignall, P.B., Widdowson, M., Ali, J.R., Jiang, H.S., Wang, W., Yan, C.B., Bond, D.P., Védrine, S., 2010. Dating the onset and nature of the Middle Permian Emeishan large igneous province eruptions in SW China using conodont biostratigraphy and its bearing on mantle plume uplift models. Lithos 119, 20–33.

Taylor, S.R., McLennan, S.M., 1985. The Continental Crust: Its Composition and Evolution. Blackwell, Oxford (312 pp.).

Thompson, G.M., Ali, J.R., Song, X.Y., Jolley, D.W., 2001. Emeishan basalts, SW China: reappraisal of the formation's type area stratigraphy and a discussion of its significance as a large igneous province. Journal of the Geological Society 158, 593–599.

Tosca, N.J., Johnston, D.T., Mushegian, A., Rothman, D.H., Summons, R.E., Knoll, A.H., 2010. Clay mineralogy, organic carbon burial, and redox evolution in Proterozoic oceans. Geochimica et Cosmochimica Acta 74, 1579–1592.

Wiedenbeck, M., Alle, P., Corfu, F., Griffin, W.L., Meier, M., Oberli, F., Quadt, A., Roddick, J.C., Spiegel, W., 1995. Three natural zircon standards for U–Th–Pb, Lu–Hf, trace element and REE analyses. Geostandards and Geoanalytical Research 19, 1–23.

Wignall, P.B., Védrine, S., Bond, D., Wang, W., Lai, X., Ali, J.R., Jiang, H., 2009. Facies analysis and sea-level change at the Guadalupian–Lopingian Global Stratotype (Laibin, South China), and its bearing on the end-Guadalupian mass extinction. Journal of the Geological Society 166, 655–666.

Winchester, J.A., Floyd, P.A., 1977. Geochemical discrimination of different magma series and their differentiation products using immobile elements. Chemical Geology 20, 325–343.

Xiao, L., Xu, Y.G., Chung, S.L., He, B., Mei, H., 2003. Chemostratigraphic correlation of Upper Permian lavas from Yunnan Province, China: extent of the Emeishan large igneous province. International Geology Review 45, 753–766.

Xiao, L., Xu, Y.G., Mei, H.J., Zheng, Y.F., He, B., Pirajno, F., 2004. Distinct mantle sources of low-Ti and high-Ti basalts from the western Emeishan large igneous province, SW China: implications for plume-lithosphere interaction. Earth and Planetary Science Letters 228, 525–546.

Xu, Y.G., Chung, S.L., Jahn, B.M., Wu, G.Y., 2001. Petrologic and geochemical constraints on the petrogenesis of Permian–Triassic Emeishan flood basalts in southwestern China. Lithos 58, 145–168.

Xu, Y.G., Luo, Z.Y., Huang, X.L., He, B., Xiao, L., Xie, L.W., Shi, Y.R., 2008. Zircon U–Pb and Hf isotope constraints on crustal melting associated with the Emeishan mantle plume. Geochimica et Cosmochimica Acta 72, 3084–3104.

Xu, Y.G., Chung, S.L., Shao, H., He, B., 2010. Silicic magmas from the Emeishan large igneous province, Southwest China: petrogenesis and their link with the end-Guadalupian biological crisis. Lithos 119, 47–60.

Yang, J.H., Cawood, P.A., Du, Y.S., Huang, H., Huang, H.W., Tao, P., 2012. Large Igneous Province and magmatic arc sourced Permian–Triassic volcanogenic sediments in China. Sedimentary Geology 261-262, 120–131.

Yang, J.H., Cawood, P.A., Du, Y.S., Huang, H., Hu, L.S., 2014. A sedimentary archive of tectonic switching from Emeishan Plume to Indosinian orogenic sources in SW China. Journal of the Geological Society 171, 269–280.

Yang, J.H., Cawood, P.A., Du, Y.S., 2015. Voluminous silicic eruptions during late Permian Emeishan igneous province and link to climate cooling. Earth and Planetary Science Letters 432, 166–175.

Zhang, L., Zhang, N., Xia, W., 2007. Conodont succession in the Guadalupian–Lopingian boundary interval (upper Permian) of the Maoershan section, Hubei Province, China. Micropaleontology 53, 433–446.

Zhang, Y., Ren, Z.Y., Xu, Y.G., 2013. Sulfur in olivine-hosted melt inclusions from the Emeishan picrites: implications for S degassing and its impact on environment. Journal of Geophysical Research: Solid Earth 118, 4063–4070.

Zheng, L.D., Yang, Z.Y., Tong, Y.B., Yuan, W., 2010. Magnetostratigraphic constraints on two-stage eruptions of the Emeishan continental flood basalts. Geochemistry, Geophysics, Geosystems 11, Q12014.

Zhong, Y.T., He, B., Mundil, R., Xu, Y.G., 2014. CA-TIMS zircon U–Pb dating of felsic ignimbrite from the Binchuan section: implications for the termination age of Emeishan large igneous province. Lithos 204, 14–19.

Zhou, M.F., Malpas, J., Song, X.Y., Robinson, P.T., Sun, M., Kennedy, A.K., Lesher, C.M., Keays, R.R., 2002. A temporal link between the Emeishan large igneous province (SW China) and the end-Guadalupian mass extinction. Earth and Planetary Science Letters 196, 113–122.

Zhou, M.F., Zhao, J.H., Qi, L., Su, W., Hu, R., 2006. Zircon U–Pb geochronology and elemental and Sr–Nd isotope geochemistry of Permian mafic rocks in the Funing area, SW China. Contributions to Mineralogy and Petrology 151, 1–19.